FFI RAPPORT

PENETRATION INTO CONCRETE - Analysis of small scale experiments with 12 mm projectiles

SJØL Henrik, TELAND Jan Arild, KALDHEIM Øyvind

FFI/RAPPORT-2002/04867

FFIBM/766/130

Approved
Kjeller 9 December 2002

Bjarne Haugstad
Director of Research

PENETRATION INTO CONCRETE - Analysis of small scale experiments with 12 mm projectiles

SJØL Henrik, TELAND Jan Arild, KALDHEIM Øyvind

FFI/RAPPORT-2002/04867

FORSVARETS FORSKNINGSINSTITUTT
Norwegian Defence Research Establishment
P O Box 25, NO-2027 Kjeller, Norway

FORSVARETS FORSKNINGSINSTITUTT (FFI)
Norwegian Defence Research Establishment

P O BOX 25
N0-2027 KJELLER, NORWAY

UNCLASSIFIED

SECURITY CLASSIFICATION OF THIS PAGE
(when data entered)

REPORT DOCUMENTATION PAGE

1) PUBL/REPORT NUMBER	2) SECURITY CLASSIFICATION	3) NUMBER OF PAGES
FFI/RAPPORT-2002/04867	UNCLASSIFIED	25
1a) PROJECT REFERENCE	**2a) DECLASSIFICATION/DOWNGRADING SCHEDULE**	
FFIBM/766/130	-	

4) TITLE

PENETRATION INTO CONCRETE - Analysis of small scale experiments with 12 mm projectiles

5) NAMES OF AUTHOR(S) IN FULL (surname first)

SJØL Henrik, TELAND Jan Arild, KALDHEIM Øyvind

6) DISTRIBUTION STATEMENT

Approved for public release. Distribution unlimited. (Offentlig tilgjengelig)

7) INDEXING TERMS

IN ENGLISH:	IN NORWEGIAN:
a) Penetration	a) Penetrasjon
b) Concrete	b) Betong
c) Experiments	c) Eksperimenter
d)	d)
e)	e)

THESAURUS REFERENCE:

8) ABSTRACT

The analytical approach for predicting penetration of rigid projectiles into concrete targets indicates that the scaled penetration depth is a function of only two non-dimensional parameters. This report analyses experiments performed to verify this relationship. In total 52 shots with 12 mm projectiles were fired against targets of standard concrete. Seven different projectiles with various masses and nose shapes were used. The experimental results seem to agree well with analytical theory. The experiments were also simulated using Autodyn-2D.

9) DATE	AUTHORIZED BY	POSITION
	This page only	
9 December 2002	Bjarne Haugstad	Director of Research

ISBN-82-464-0734-1

UNCLASSIFIED

SECURITY CLASSIFICATION OF THIS PAGE
(when data entered)

CONTENTS

PENETRATION INTO CONCRETE - Analysis of small scale experiments with 12 mm projectiles

Preface

This report was originally written in 2000 with report number 2000/04414, but the final publication was, due to priority considerations, postponed to 2002. The report was therefore given a new number 2002/04867. If one tries to search for the old number, a reference to this document is still found.

1 INTRODUCTION

As shown in Teland [1], the existing empirical formulas for predicting penetration into concrete give different results for the same problem. Some of this difference is due to the range of parameters used in the various experiments, see Sjøl & Teland [2], and Teland & Sjøl [3], and the fact that too many parameters have been varied at the same time trying to produce one single empirical formula.

Forrestal's formula [4-8] seems to be in good agreement with most of the experimental results we have examined so far [2]. On writing this formula on non-dimensional form, the penetration depth is seen to depend only on two non-dimensional parameters [2]. To verify this relationship, it was decided to perform some further experiments. Hence, a large range of the slimness parameter M/N (see Chapter 2 for details) was used in the experiments. The projectiles were chosen to correspond to modern penetrators, as described in Lausund et al [9].

Experiments with small targets diameters have been shown to result in larger penetration depths than predicted by Forrestal's formula [10]. The reason for this is boundary effects, so to avoid such problems, a sufficienly large target diameter was chosen.

For many of the existing penetration data in the literature, only a few properties of the concrete targets are known, usually the compressive strength and the density. When analysing the concrete in hydrocodes, a more complete concrete model is needed. We therefore performed triaxial material tests to obtain relevant material parameters. The results from triaxial material tests give input data to the numerical simulations described in Chapter 5.

2 THEORETICAL BACKGROUND

Forrestal's formula is based on spherical cavity expansion theory, and the penetration depth is given by

$$X = \frac{2}{\pi}\frac{M}{N}\ln\left(\frac{\hat{V}^2 + M/N}{\pi/2 + M/N}\right) + 2 \tag{2.1}$$

where

$$X = \frac{x}{d} \quad M = \frac{m}{d^3\rho_t} \quad \hat{V} = \frac{V}{\sqrt{S}} = \sqrt{\frac{m}{Sd^3\sigma_c}}v \quad N = \frac{8(r/d)-1}{24(r/d)^2} \tag{2.2}$$

The parameter S was originally calibrated to Forrestal's experiments, but was later modified by Sjøl & Teland [2] to cover a larger range of concretes, including compressive strengths up to 200 MPa. The modified S-factor is defined as

$$S = 49.5\left(\frac{\sigma_c}{10^6}\right)^{-0.43} \tag{2.3}$$

Equation (2.3) is used for the S-factor in the analysis of the experimental data in Chapter 4.

The penetration formula based on cavity expansion theory is available in several versions. The original Forrestal's formula, as given by Equation (2.1), is the basic formula. In [11], a modified version based on different nose geometries can be found. A special case of this approach is flat nosed projectiles, where the maximum penetration depth into concrete targets is seen to be [2]

$$X = \frac{2}{\pi}M\ln\left(1 + \frac{1}{M}\hat{V}^2\right) \tag{2.4}$$

Real projectiles do not have flat noses, but some may have a flat, truncated, part of the nose. Analysis and discussion of such projectiles can be found in Teland & Sjøl [11]. The flat nose approach given here may be valid for small fragments, and is also a "limit case" for the application of the modified formula.

We see from Equation (2.1) or Equation (2.4) that the scaled penetration depth only depends on two non-dimensional parameters, namely $\hat{V}$ (scaled impact velocity) and M/N ("slimness parameter"). In Figure 2.1, the scaled penetration depth as a function of the scaled impact velocity is shown for different values of the "slimness parameter". The range of the "slimness parameter" is similar to the values used in the experiments described in this report.

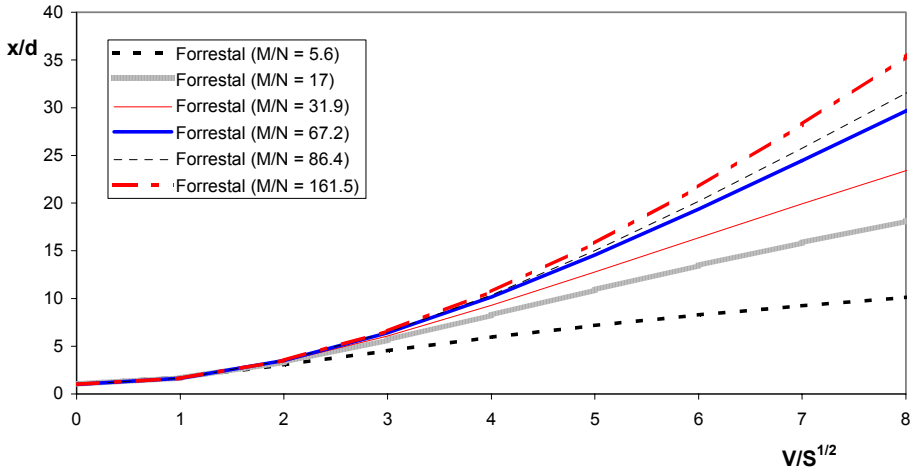

Figure 2.1: The maximum penetration depth given by Forrestal's formula for the projectiles analysed in the experiments.

It is seen in Figure 2.1 that the value of the slimness parameter *M/N* is important, especially for large scaled impact velocities.

3 EXPERIMENTAL SETUP

In order to verify the theoretical calculations described in Chapter 2, the following experiments were performed. We used a modified 12.7 mm gun, which was the same as used in the previous experiments [10]. For velocity measurement, 2 coils connected to an oscilloscope with a mutual distance of 1 meter were used. The projectiles were therefore magnetized before they were fired. The distance from the gun to the target was 5 meters in the first experiments, but when instability of the projectile was discovered, this distance was reduced to 2 meters from shot number 58 and onwards.

Figure 3.1: Experimental set-up.

4 RESULTS

The numbering of the shots is continued from our previous experiments [10]. Shot number 41 to 49 were used to test the gun, and were fired without any target. Therefore the experimental results start with shot number 50. All experimental results are summarized in Tables 4.1 and 4.2. In these tables, "*X_F*" denotes the non-dimensional penetration depth calculated by Equation (2.1) for ogive nosed projectiles and Equation (2.4) for flat nosed projectiles. Deviation between experimental and theoretical penetration depth, given by either Equation (2.1) or (2.4) is also shown. For different reasons, some quantities were not measured. Such cases are denoted by a '-' in the tables.

In Figure 4.1, the projectiles used in the experiments are shown, and in Figure 4.2, the targets after penetration from shot number 65 and 77 are shown.

1	20.5 g steel
2	24.2 g steel
3	51.1 g tungsten
4	65.8 g tungsten
5	65.7 g tungsten
6	122.8 g tungsten

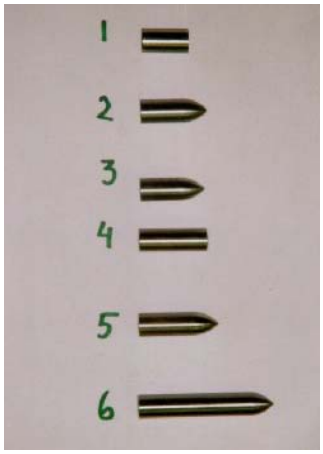

Figure 4.1: Projectiles used in the experiments. In addition, a flat-nosed version of the 122 g projectile was used.

Figure 4.2: Pictures from shot number 65 and 77.

Table 4.1: Experiments with flat nosed projectiles.

									Crater	
Shot	**m**	**M/N**	**Gun**	**v**	**x**	**X**	**X_F**	**Deviation**	**Diameter**	**Depth**

#	[g]		powder [g]	[m/s]	[mm]			[%]	[mm]	[mm]
50	20,5	5,4	8	654	48	4,0	4,3	-7,2	140	-
51	20,5	5,4	6	498	43	3,6	3,1	16,3	100	-
52	20,5	5,4	4	368	27	2,3	2,0	12,2	100	-
80	122,28	32,2	8	405	147	12,3	13,8	-11,2	120	26
82	65,24	17,2	8	505	126	10,5	10,0	5,1	150	32
83	65,94	17,4	6	434	123	10,3	8,2	24,8	120	28
84	65,83	17,3	4	312	71	5,9	5,0	18,9	110	33
85	65,82	17,3	10	614	171	14,3	12,9	10,8	200	30
86	65,94	17,4	13	680	206	17,2	14,5	18,6	135	30
87	65,14	17,1	5	362	91	7,6	6,2	22,0	90	26
88	122,56	32,2	3	219	60	5,0	5,1	-1,7	120	25
89	122,96	32,3	5	288	93	7,8	8,2	-5,0	80	21
90	122,28	32,2	7	361	147	12,3	11,6	5,4	170	22
95	123,22	32,4	6	329	125	10,4	10,1	2,7	80	21
99	64,79	17,0	4,5	356	75	6,3	6,0	3,7	100	22

Table 4.2: Experiments with ogive nosed projectiles.

									Crater	
Shot #	**m [g]**	**M/N**	**Gun powder [g]**	**v [m/s]**	**x [mm]**	**X**	**X_F**	**Deviation [%]**	**Diameter [mm]**	**Depth [mm]**
53	25	32,9	7	567	71	5,9	7,7	-23,3	125	-
54	25	32,9	4	359	20	1,7	4,0	-58,0	80	-
55	25	32,9	6	506	30	2,5	6,5	-61,6	95	-
56	24,22	31,9	6	506	67	5,6	6,4	-12,0	140	-
57	24,21	31,8	4	414	23	1,9	4,7	-59,5	-	-
58	24,01	31,6	4	436	48	4,0	5,1	-21,1	130	26
59	24,25	31,9	10	810	158	13,2	12,6	4,4	140	27
60	24,22	31,9	8	643	116	9,7	9,0	7,0	125	20
61	24,3	32,0	6	500	85	7,1	6,3	13,3	165	26
62	51,11	67,2	5	398	107	8,9	8,3	7,4	130	25
63	50,84	66,9	3	305	68	5,7	5,4	4,6	90	25
64	50,22	66,1	7	512	158	13,2	12,3	7,2	105	25
65	50,36	66,2	10	664	224	18,7	18,6	0,5	90	22
66	51,08	67,2	2	245	64	5,3	3,9	36,1	125	25
67	50,4	66,3	12	707	-	-	20,5	-	-	-
68	50,64	66,6	13	828	-	-	26,0	-	-	-
69	65,72	86,4	7	482	178	14,8	14,3	4,0	130	26
70	65,97	86,8	10	614	251	20,9	21,2	-1,5	130	19
71	65,3	85,9	3	275	72	6,0	5,7	6,1	80	22
72	66,28	87,2	13	702	212	17,7	26,3	-32,9	200	30
73	66,1	86,9	13	699	320	26,7	26,1	2,3	100	24
74	63,23	83,2	17	799	162	13,5	30,6	-55,9	125	23
75	65	85,5	17	734	217	18,1	27,7	-34,6	190	35
76	66,28	87,2	5	373	108	9,0	9,4	-4,2	115	24
77	122,8	161,5	8	381	186	15,5	17,2	-9,7	145	20
78	123,53	162,5	12	526	345	28,8	30,1	-4,4	150	24
79	124,68	164,0	16	576	322	26,8	35,3	-24,0	120	39
81	124,28	163,5	25	747	-	-	53,4	-	-	-
91	123	161,8	3	198	77	6,4	5,6	13,9	130	22
92	123,44	162,4	5	264	109	9,1	9,1	-0,4	150	22
93	23,87	31,4	6	564	108	9,0	7,4	22,3	120	22
94	51,17	67,3	4	358	82	6,8	7,0	-2,5	105	27
96	123,46	162,4	7	353	181	15,1	15,1	-0,1	70	20
97	124,58	163,9	10	458	252	21,0	23,9	-12,3	160	17
98	50,62	66,6	12	742	279	23,3	22,1	5,1	160	22
100	123,05	161,8	16	616	378	31,5	38,9	-19,1	100	27
101	65,84	86,6	15	754	299	24,9	29,2	-14,6	150	24

4.1 Analysis of results

4.1.1 Ogive nosed projectiles

The penetration depth for the ogive nosed projectiles, as shown in Table 4.2, are in Figure 4.3 compared to Forrestal's formula.

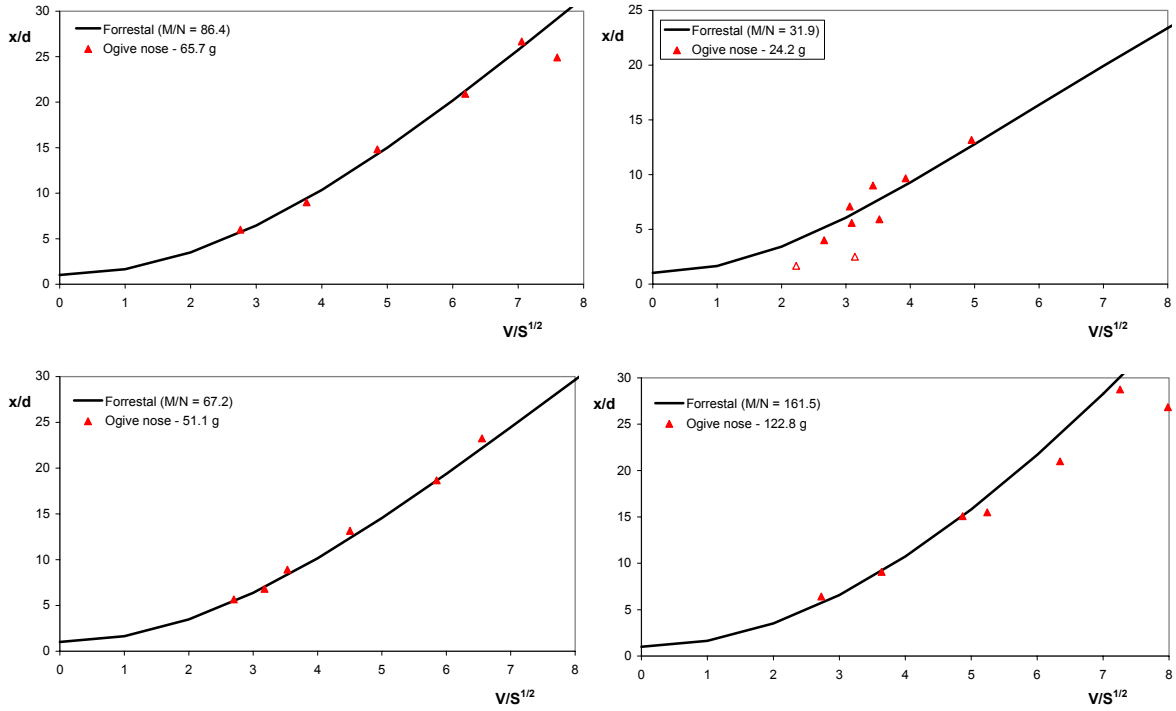

Figure 4.3: Experiments with ogive projectiles compared to Forrestal's formula. The open triangles indicate experiments with oblique impact, which can therefore not be compared directly with Forrestal's formula.

The experiments show good agreement with Forrestal's formula for different values of *M/N* for ogive nosed projectiles. Some experiments give, however, too low values for the penetration depth compared to the predicted value. Due to some flight instabilities of the projectile, some of the 24.2 gram penetrators did not hit the target with a 90 degree angle. In the cases where the deviation from "normal impact" was 10-15 degrees, the penetration depth was observed to be smaller than expected. These experiments are shown with open triangles in Figure 4.3. For the two largest penetrators, the projectile trajectory inside the concrete target was observed to be curved in the final phase of the penetration process for high impact velocities. It was therefore difficult to measure the exact penetration depth. The real penetration depth in these cases should be somewhat larger, and hence be closer to the theoretical value calculated by Forrestal's formula.

4.1.2 Flat nosed projectiles

The penetration depth for the flat nosed projectiles, as shown in Table 4.1, are in Figure 4.4 compared to the theoretical models given by Equation (2.1) and Equation (2.4).

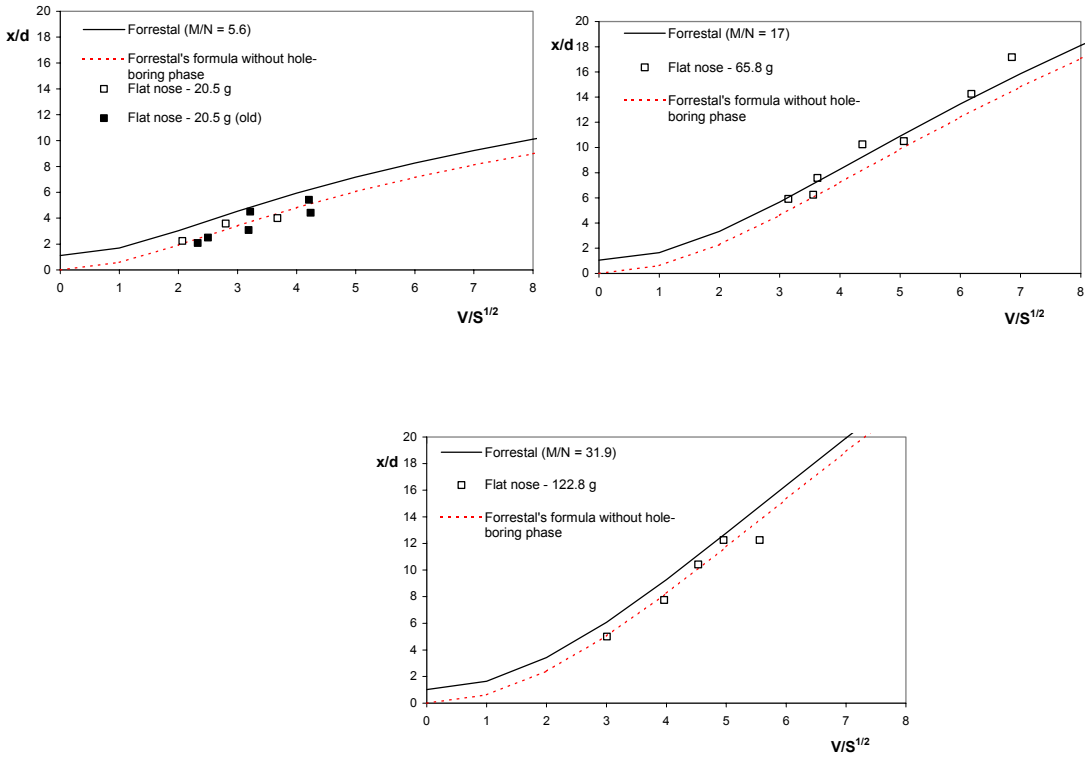

Figure 4.4: Experiments with flat projectiles compared to Forrestal's formula and the modified formula for flat nosed projectiles.

The hole-boring phase is in Teland & Sjøl [11] defined as the penetration of the nose, while in Forrestal's approach it is defined for penetration depths less than two calibres. Our approach, using the nose length as the transition between the cratering and tunnelling phases seems more natural from a physical point of view. The experiments with the 24.1 gram and the 122.8 gram projectiles, as shown in Figure 4.4, also seem to support the new model. However, for the 65.8 gram projectiles the experimental results agree better with the original Formula (2.1). The reason for this is unclear.

4.1.3 Constant *M/N* – different nose shape

The flat nosed 122 g projectiles and the ogive nosed 24 g projectiles have approximately the same value of *M/N*, and hence, should give approximately the same penetration depth according to Forrestal's formula. These experiments are in Figure 4.5 compared to each other and to Forrestal's formula. We see from Figure 4.5 that projectiles with ogive noses result in larger penetration depth than flat nosed projectiles for constant value of the slimness parameter. Here we see the strength of using non-dimensional parameters. Although the mass of the flat nosed projectile is approximately 5 times the mass of the ogive projectile, according to Forrestal, the penetration depth should have been equal in these two cases. However, in the experiments, the penetration depth for the flat nosed projectiles was slightly smaller than for the ogive nosed projectiles, again supporting our modified theory.

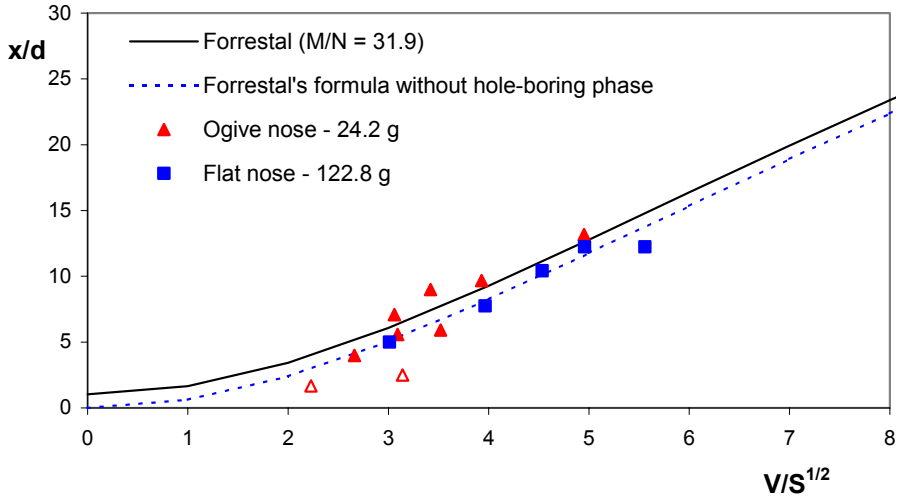

Figure 4.5: Experiments with ogive nosed 24.2 grams projectiles and 122.8 flat nosed projectiles compared to Forrestal's formula. The open triangles mean oblique impact.

4.1.4 Constant mass – different nose shape

The projectiles with mass of 65 grams and 122 grams had either a flat or an ogive nose. In Figure 4.6, the penetration depth for projectiles with constant mass but different nose shape are compared. Based on the discussion in Section 4.1.3,and the results in Figure 4.6, we clearly see the difference between the penetration capability of flat and ogive nosed projectiles.

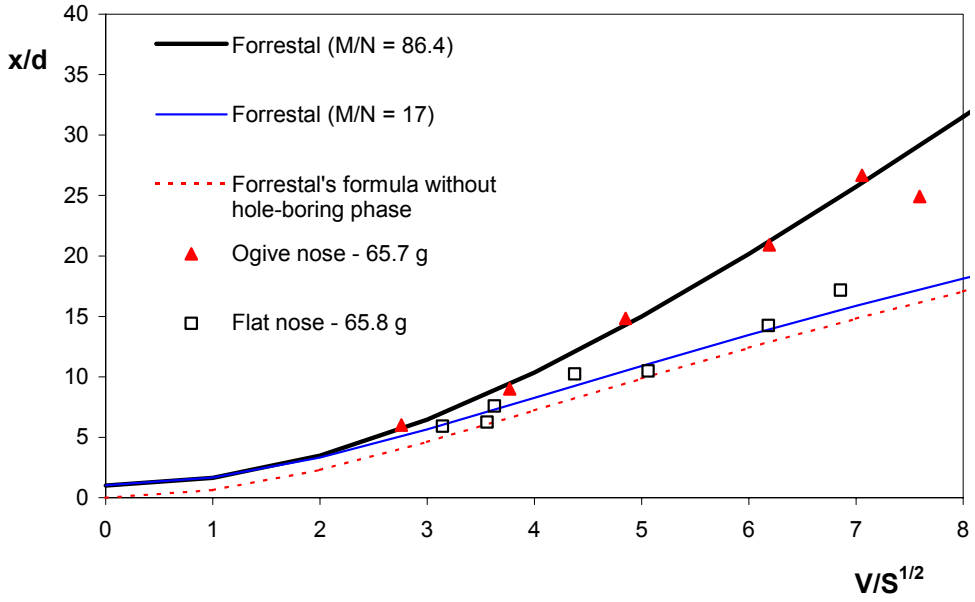

Figure 4.6: Penetration depth for projectiles with mass 65.8 g with different nose shape.

4.1.5 One empirical formula?

Most of the existing empirical formulas for predicting penetration into concrete are based on a wide range of experiments. Without any knowledge of the physics involved in the problem, one normally tries to perform curve fitting of all the data. In Figure 4.7, the penetration depth as a function of scaled impact velocity for all experiments are shown. It might have been natural to try constructing a relationship between X and V based on curve-fitting to these data points.

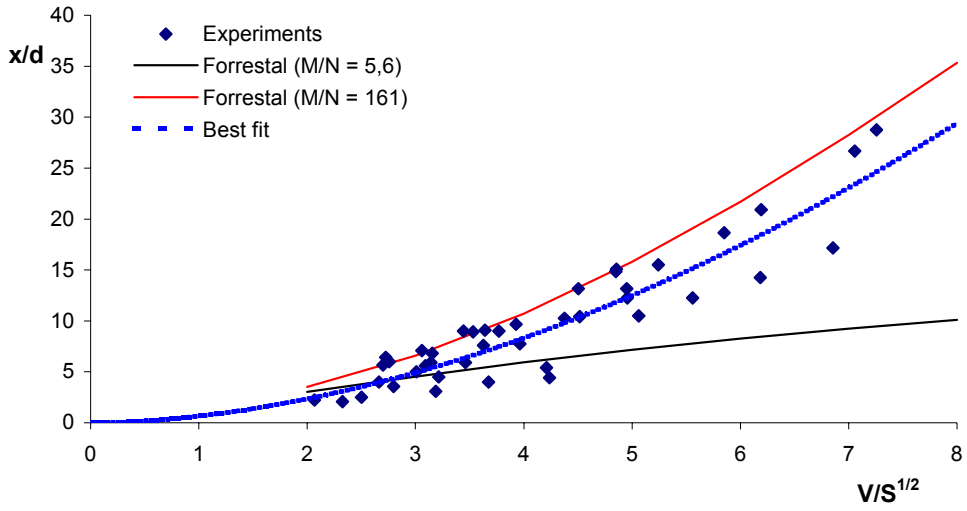

Figure 4.7: All experimental data compared to Forrestal's formula for M/N = 5.6 and 161, respectively, and a best fit.

However, without any knowledge of Forrestal's formula and cavity expansion theory, it would be almost impossible to guess how *M/N* should be included in the analysis[1]. The "best fit" curve shown in Figure 4.7 gives an "average" value of the penetration depth. For projectiles with "average" values of the slimness parameter *M/N*, the empirical formula may give acceptable results, but if for instance slim penetrators are used, the "empirical average" will be inadequate to predict the final penetration depth.

This example illustrates that one should be very careful finding empirical relations with only a modest knowledge of the physics and theory behind the problem studied, especially if too many parameters are varied simultaneously.

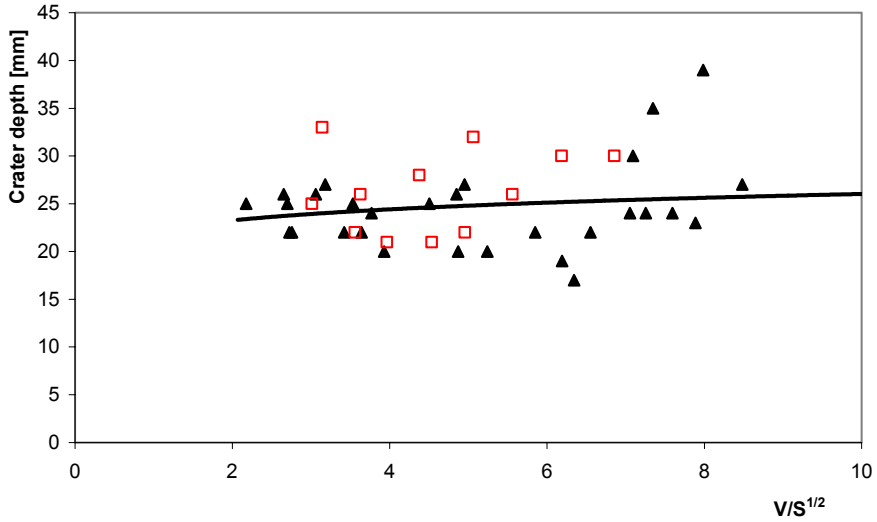

Figure 4.8: Crater depth as a function of scaled impact velocity ("triangles" are results from experiments with ogive nosed projectiles and "squares" are results from experiments with flat nosed projectiles). The solid line is a least square approximation to all experimental data.

[1] The *S*-factor, which is a material constant, is of course also a parameter which requires knowledge of cavity expansion theory, but since all experiments discussed here are performed against targets of identical concrete, the S-factor is identical in all experiments.

4.2 Crater depth

The crater depth is varying from 17 to 39 mm for the experiments, with a mean value of approximately 2 calibres (24 mm). In Figure 4.8, the crater depth as a function of impact velocity is shown for the different projectiles used in the experiments. There seems to be a large scattering of the experimental data, which makes it difficult to develop a model without further investigations.

4.3 Crater diameter

Figure 4.9 shows the crater diameter as a function of impact velocity for the different projectiles used in the experiments. Again, large scattering makes it difficult to analyse the data.

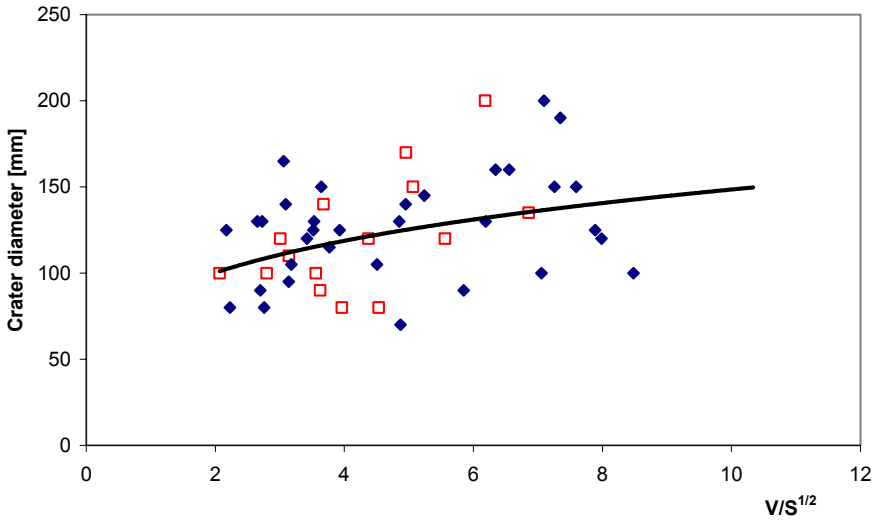

Figure 4.9: Crater diameter as a function of scaled impact velocity ("triangles" are results from experiments with ogive nosed projectiles and "squares" are results from experiments with flat nosed projectiles). The solid line is a least square approximation to all experimental data.

5 NUMERICAL SIMULATIONS

The experiments described in this report have been simulated numerically, using Autodyn-2D, version 4.1.13. The main focus in these simulations has been to verify the influence of the slimness parameter. Axis-symmetry has been utilized, and the problem was modelled using a Lagrangian projectile and a Eulerian target. The concrete used in the target material were tested tri-axially, and material data for a simple Mohr-Coulomb model was obtained. This model is described more closely in the next section.

There exist more complex material models in Autodyn, like the RHT-model, which can be used for concrete materials. These, however, require a large amount of input parameters, which we have no experimental data for. Generating such material data was considered to be beyond the scope of the present report, and was therefore not investigated any further. The Mohr-Coulomb model was, however, considered to be sufficient for the present analysis.

5.1 Porous Mohr-Coulomb material model

Concrete specimens were analysed in a GREAC cell to produce triaxial material data for the concrete to be used in Autodyn simulations. In [13], a procedure for converting the GREAC cell results to Mohr-Coulomb data is described, and in Table 5.1, the Porous Mohr-Coulomb model used in the Autodyn-simulations is shown.

Table 5.1: Porous Mohr-Coulomb material model for the 35 MPa concrete used in the Autodyn simulations.

Equation of state		Mohr-Coulomb	
Density [kg/m^3]	Pressure [MPa]	Pressure [MPa]	Yield strength [MPa]
2186	11	0	12
2270	62	12	36
2370	142	83	97
2426	300	162	126
2472	556		

In addition, the following parameters are needed:

Shear modulus: 4826 MPa
Reference density: 2395 kg/m^3
Solid Sound Speed: 2636 m/s
Porous Sound Speed: 1429 m/s
Hydrodynamic tensile limit (P_{min}) -4 MPa

5.2 Simulation results

In the numerical simulations, we have focused on the final penetration depth, and compared these values to the analytical and experimental results. The penetration results obtained from Autodyn-2D are shown in Tables 5.2 – 5.3, and in Figures 5.1 – 5.2. The numerical simulations seem to give larger penetration depth compared to both experiments and theoretical calculations.

This indicates that the concrete model used in the simulations is somewhat "softer" than the concrete used in the experiments. As pointed out earlier, only a simple material model has been used, so perfect agreement with experiments might not be expected. Possible sources of error include not accounting for that the GREAC cell test produces material data for slightly damaged concrete, as the concrete specimen is gradually damaged during the material test. Strain rate effects were also not implemented in the material model, as these are slightly controversial. These effects, if included, would have made the concrete model stronger, and therefore reduced the penetration depth, giving better agreement with experiments. Nevertheless, the numerical simulations show a similar M/N-relationship than found analytically and by experiments.

Table 5.2: Simulation results for ogive nosed projectiles.

Projectile mass [g]	Impact velocity [m/s]	Penetration depth [mm]
25	300	48
	400	71
	480	93
	600	132
51	200	46
	300	81
	400	126
	500	180
	600	248
	700	326
65	200	46
	300	81
	400	126
	500	180
	600	248
	700	326
123	200	86
	275	142
	350	216
	425	307
	500	414

Table 5.3: Simulation results for flat nosed projectiles.

Projectile mass [g]	Impact velocity [m/s]	Penetration depth [mm]
20.5	200	12
	300	22
	400	35
	500	48
	600	62
	700	76
	800	89
65	300	62
	400	100
	500	144
	600	190
123	200	55
	300	110
	400	180

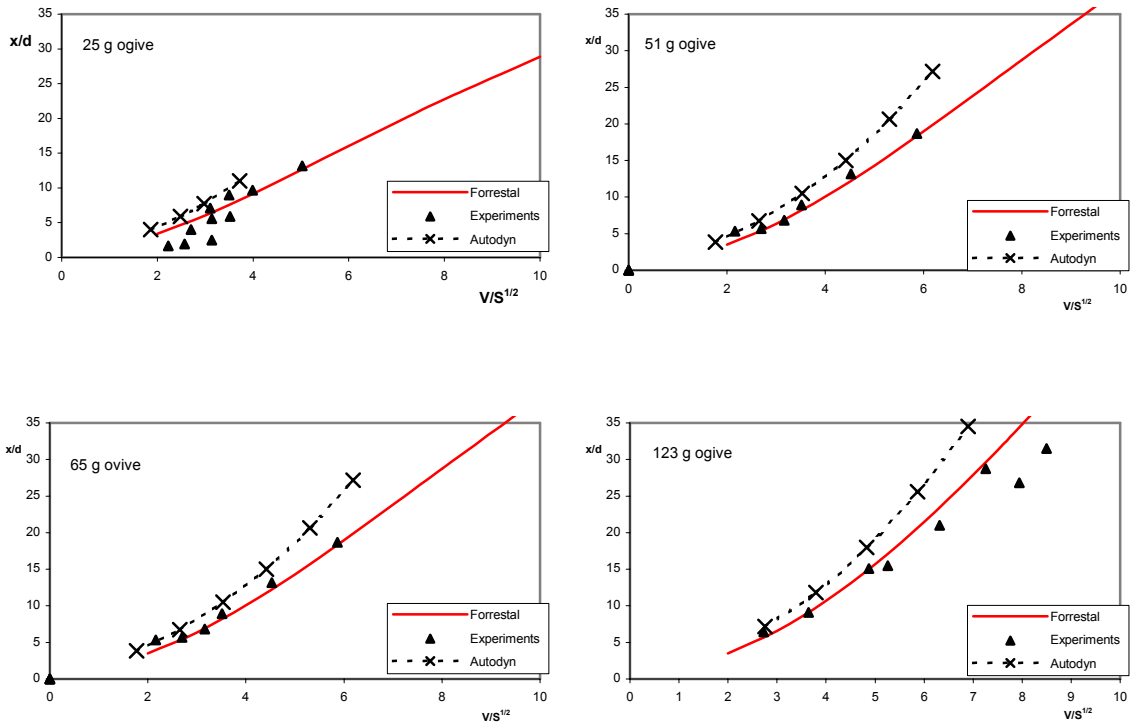

Figure 5.1: Comparison between Autodyn-simulations, experiments and Forrestal's formula for ogive nosed projectiles.

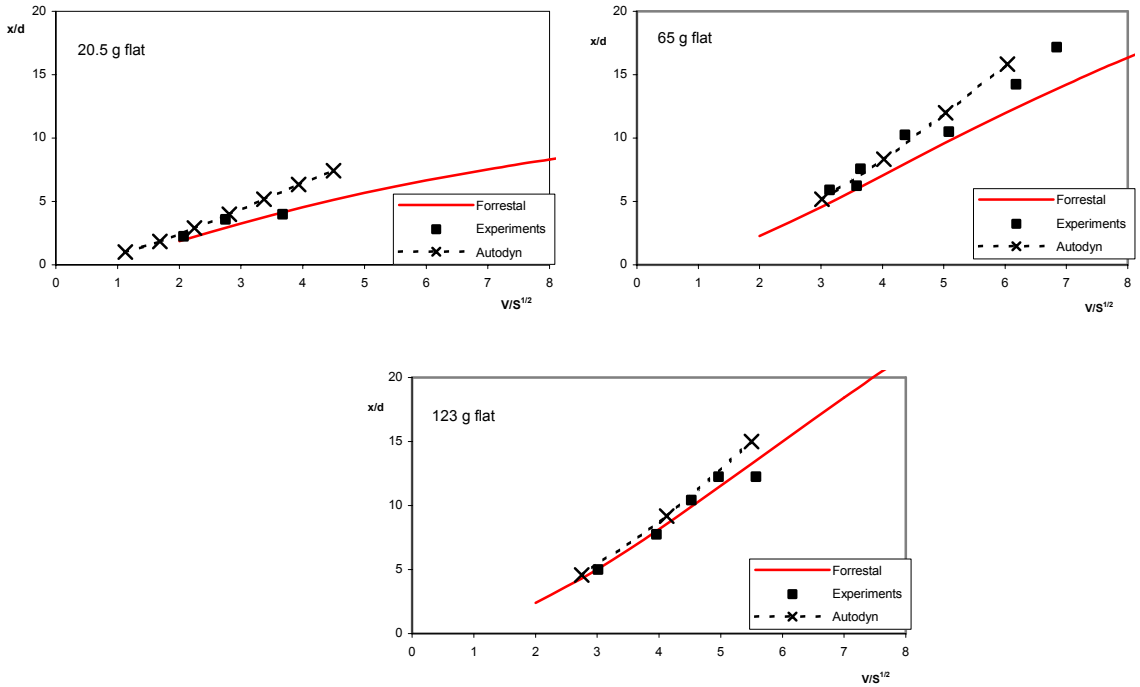

Figure 5.2: Comparison between Autodyn-simulations, experiments and Forrestal's formula for flat nosed projectiles.

6 CONCLUSIONS

The penetration depth found experimentally seems to be in good agreement with Forrestal's formula. Projectiles with the same *M/N*, but different nose shape, seem to give the same relationship between impact velocity and penetration depth, both theoretically and experimentally. This emphasizes the value of describing a problem in terms of non-dimensional parameters in order to achieve a deeper understanding. The analysis in Section 4.1.5 shows that it is necessary to know the physics of the problem if one attempts to make empirical relations when varying many parameters simultaneously.

The numerical simulations seem to give larger penetration depth than the experiments, which may be due to the simple material model used. By using more sophisticated material models (which we of course are capable of, but which is beyond the scope of this report), it should be possible to model the concrete behaviour more accurately.

APPENDIX

A KINETIC ENERGY OF THE PROJECTILES

In the experiments, gunpowder of the type "Vihta Vouri Oy 160" were used, and in Tables 4.1 and 4.2, the amount of gunpowder for each shot is given. In Figure A.1, the relationship between the amount of gunpowder used and kinetic energy of the projectiles is shown. It is seen that the heaviest projectiles achieve higher kinetic energy compared to the lightest projectiles for the same amount of gunpowder. This is due to the combustion properties of the gunpowder.

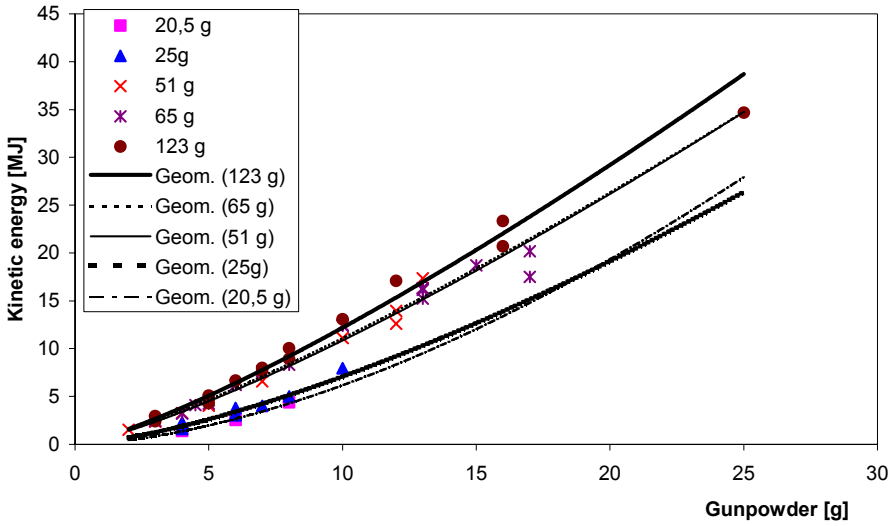

Figure A.1: Relationship between mass of gunpowder and kinetic energy for the projectiles used in the experiments.

References

(1) Teland J A (1997): A review of empirical equations for missile impact effects on concrete, FFI/RAPPORT/05856

(2) Sjøl H (1999): Prediction of concrete penetration using Forrestal's formula, FFI/RAPPORT-99/04415

(3) Teland J A, Sjøl H (1999): An examination and reinterpretation of experimental data behind various empirical equations for penetration into concrete, *Proceedings of the 9th international symposium on interaction of the effects of munition with structures, 3-7 May 1999, Berlin Germany*, 267 - 274.

(4) Forrestal M J, Luk V K (1992): Penetration into soil targets, *Int J of Impact Eng* **12**, 427 - 444.

(5) Forrestal M J, Altman B S, Cargile J D, Hanchak S J (1994): An empirical equation for penetration depth of ogive nose projectiles into concrete targets, *Int J Impact Eng* **15**, 4, 395-405.

(6) Forrestal M J, Frew D J, Hanchak S J, Brar N S (1996): Penetration of grout and concrete targets with ogive-nose steel projectiles, *Int J Impact Eng* **18**, 5, 465-476.

(7) Frew D J, Hanchak S J, Green M L, Forrestal M J (1998): Penetration of concrete targets with ogive-nosed steel rods, *Int J Impact Eng* **21**, 6, 489-497.

(8) Luk V K, Forrestal M J (1987): Penetration into semi-infinite reinforced concrete targets with sperical and ogival nose projectiles, *Int J Impact Eng* **6**, 4, 291-301.

(9) Lausund R, Blanch J H, Høybråten S, Skjervold J E (1999): (U) Teknisk trussel mot stasjonære anlegg, FFI/RAPPORT-99/05858 (Restricted, in Norwegian)

(10) Teland J A, Sjøl H (2000): Boundary effects in penetration into concrete, FFI/RAPPORT-2000/05414

(11) Teland J A, Sjøl H (2000): Penetration into concrete by truncated projectiles, FFI/RAPPORT-2000/05292

(12) Sjøl H, Teland J A, Kaldheim Ø (1998): Penetrasjon i betong med 12 mm prosjektiler, FFI/NOTAT-98/04392 (in Norwegian)

(13) Rusås P-O, Teland J A (2000): Matlab toolbox for prosessing of GREAC cell data, FFI/RAPPORT-2000/02032

DISTRIBUTION LIST

FFIBM **Dato:** 9 December 2002

RAPPORTTYPE (KRYSS AV)	RAPPORT NR.	REFERANSE	RAPPORTENS DATO
X RAPP ☐ NOTAT ☐ RR	2002/04867	FFIBM/766/130	9 december 2002
RAPPORTENS BESKYTTELSESGRAD		ANTALL EKS UTSTEDT	ANTALL SIDER
Unclassified		21	25
RAPPORTENS TITTEL		FORFATTER(E)	
PENETRATION INTO CONCRETE - Analysis of small scale experiments with 12 mm projectiles		SJØL Henrik, TELAND Jan Arild, KALDHEIM Øyvind	
FORDELING GODKJENT AV FORSKNINGSSJEF:		FORDELING GODKJENT AV AVDELINGSSJEF:	

EKSTERN FORDELING

ANTALL	EKS NR	TIL
1		Øyvind Kaldheim 5590 Etne

INTERN FORDELING

ANTALL	EKS NR	TIL
9		FFI-Bibl
1		FFI-ledelse
1		FFIE
1		FFISYS
1		FFIBM
1		FFIN
3		Forfattereksemplar(er)
3		Restopplag FFI-bibl
		Elektronisk fordeling:
		FFI-veven
		Haakon Fykse (HFy)
		Svein E Martinussen (SEM)
		John F Moxnes (JFM)
		Ove Dullum (OSD)
		Knut B Holm (KBH)